MHD Stagnation Point Flow of Ternary Hybrid Nanofluid Flow over a Stretching/Shrinking Cylinder with Suction and Ohmic Heating

Zafar Mahmood [1], Umar Khan[2,] *

[1] Department of Mathematics and Statistics, Hazara University, Mansehra, Pakistan, zafarmaths222@gmail.com

[2] Department of Mathematics and Statistics, Hazara University, Mansehra, Pakistan, umar_jadoon4@yahoo.com

* *Correspondence: umar_jadoon4@yahoo.com ; Tel.: +92-332-890-2728*

Abstract: There is a new type of nanofluid called ternary hybrid nanofluid that can be used to improve heat flow. This study investigates effects of magnetic field, mass suction with ohmic heating towards stagnation region of stretching/shrinking cylinder of polymer based ternary hybrid nanofluid flows in two dimensions with different shapes aspect. Under the imposed assumptions, equations governing the flow will be modelled. It is feasible to convert nonlinear partial differential equations that are not exactly solvable via similarity transformation to a system of ordinary differential equations, which are solved numerically. The combination of Runge–Kutta-IV and shooting method in Mathematica has been shown to have a substantial impact on the prevalence of heat exchange and the mobility parameters of ternary hybrid nanofluids. The number of nanoparticles with suction enhances heat transfer and skin friction coefficient. Graphs and tables demonstrated the influence of many factors such as suction, Reynold number, nanoparticles volume fraction, magnetic field, Eckert number, stretching/shrinking on temperature, velocity, skin friction and local heat transfer rate coefficients curves. To verify the findings, a contrast study was undertaken between the current research and previously published results for a specific instance, and excellent agreement was discovered.

Keywords: Suction; stagnation point; magnetic field, Ternary hybrid nanofluid; cylinder; numerical solution

1. Introduction

Stretching/shrinking surfaces are used to research heat transfer and flow, the upshot of which is a diverse variety of valuable engineering uses, including heat retention, the production of complex synthetic structures, the production of crystal and other types of subterranean transportation systems. Industrial applications of heat transfer and flow exploration are critical since the quality of a finished product is affected by how quickly heat exchange occurs and

how quickly velocity gradients change [1], [2]. Hybrid nanofluid is a novel kind of heat transfer fluid that has the potential to outperform both standard cooling fluids (water and ethylene glycol) and nanofluids (single nanoparticle) in terms of heat transfer performance. It is well documented that hybrid nanoparticles are important in several manufacturing and technological regions and that the synthesis and constancy of hybrid nanoparticles have been studied in numerous review studies [3]–[6]. When it comes to creating a durable hybrid nanofluid, one of the most important elements to consider is choosing an appropriate blend of nanoparticles. Metal nanoparticles(Cu, Ag), metal oxides(Al_2O_3, CuO, Fe_2O_3), carbon materials (graphite, MWCNTs, CNTs), metal carbide and metal nitride were the most regularly encountered types of nanoparticles. In addition, the size, shape, and solid volume fractions of the nanoparticles are all essential aspects in optimizing the thermal conductivity of the hybrid nanofluid, as is the composition of the nanoparticles. In the description of boundary layer flow in nanofluid, the mathematical models of Buongiorno [7] and Tiwari and Das [8] are often utilized. Stretching flow using the Buongiorno model has been the subject of further studies, including [9]–[11]. Tiwari and Das model were updated to include the thermophysical features of hybrid nanofluids described by Devi and Devi [12]. Under magnetic field conditions and low suction strength($0 \leq S \leq 1.5$), the heat transfer rate of $Cu - Al_2O_3/H_2O$ hybrid nanofluid was larger than that of Cu-water nanofluid.

It is necessary to include consequences in the flow to determine if the impact contributes to the flow providing a good relevance. Suction is one of the effects that researchers are interested in examining more extensively. External flows or energy losses may be reduced by controlling the boundary layers by suction. Boundary layer separation may be prevented or hindered by this technique. The surface must have flaws, crevices, apertures, porosity regions, or perforated in order to provide the suction impact. Use these funnels to draw air from the boundary layer that moves at a slower rate near the wall. A result of this filling is a complete and strong boundary layer velocity curve when separated. For boundary layer management, Hartnett [13] identified the need of suction or injection. Reduce drag and attain high elevation values are generally achieved by swiftly impeding boundary-layer separation. Because of this, suction or injection of fluid via a surface may drastically alter the flow field, including in mass transfer cooling Several academics have played an active role in investigations on the effects of suction because of this amazing concept [14], [15] have examined the impact of suction on a variety of surfaces and fluids.

Stagnation point flow is a term used to describe the flow that separates when it comes into contact with a solid surface. At the manufacturing and technological sectors, this kind of flow

has been widely used because it has the best heat transmission, fluid pressure, and mass deposition rate in the stagnation point zone. Stagnation point flow was first described in classical works by Hiemenz [16] and Homann [17]. Chiam [18] was the first to investigate the stagnation point flow caused by a stretched flat plate, whereas Wang [19] studied a contracting sheet and found two solutions. The experiments on the stagnation point flow near deformable flat plate were afterwards undertaken by [20], [21] employing standard and hybrid nanofluids, correspondingly. Disc, wedge, and cylinder fluid flow have all been studied more thoroughly in recent years because to technological and industrial advancements. Wang [22] did some early work on fluid flow toward a stretching cylinder. Ishak and Nazar [23] found a solution for laminar boundary layer flow of a viscous fluid along a stretching cylinder that was similar to Wang's work. MHD slip flow with heat production and outward velocity was investigated by Vinita and Poply [24] using Buongiorno's nanofluids model. When it comes to viscous fluid, Najib et al [25] and Omar et al [26] looked at the stagnation point flow toward an expanding/contracting cylinder. It has recently been shown that [27] the stagnation point flow over a static cylinder may be analyzed in three dimensions and two solutions have been established [27]. $Cu - Al_2O_3/H_2O$ hybrid nanofluid has a higher heat transfer rate than Cu-water nanofluid. Iskandar Waini [28] studied the flow of hybrid nanofluids toward a stagnation point on a stretching/shrinking cylinder.

The MHD fluid flow is greatly influenced by Joule or ohmic heating, which has been one of the most intriguing effects to be imposed. Joule heating, also known as Ohmic heating, is a technique of converting electric energy into thermal energy that creates heat via resistive losses in a material throughout the conversion process. The Joule heating effect, on the other hand, is extensively and effectively exploited in the majority of electrical and electric equipment nowadays. Using a $Cu - Al_2O_3/H_2O$ hybrid nanofluid, Maskeen et al [29] studied the flow through a vertical stretched cylinder in MHD. In nanofluid flow with compliant walls, Reddy and Reddy [30] found that Joule heating had an impact. Joule heating may raise the temperature, according to the researchers, who explained this further. In the existence of Joule heating, Sajid et al [31]reported a numerical solution for MHD ferrofluid flow in a semi-porous curved channel. Stretching flow in nanofluids performing electrical MHD with Joule heating was studied by Daniel et al [32]. One of the two solutions to the MHD flow of copper alumina/water nanofluid via a permeable exponentially diminishing surface was discovered by Yan et al.[33].

Nanofluids have been the subject of a decade of study that has shown their ability to transmit heat effectively. While it is possible to improve the characteristics of mono nanofluids by

altering the volume concentration of the nanoparticle, this is limited by the difficulty in balancing the net negative of viscosity rise against the net positive of viscosity decrease. Researchers have developed hybrid nanofluids to overcome this constraint and exploit the unique features of several kinds of nanoparticles. A novel class of working fluids has been found and widely researched in recent years, consisting of three solid nanoparticles distributed in a normal fluid. This is a departure from early hybrid nanofluid experiments, which used two-particle nanofluids. 'Trihybrid nanofluids', 'ternary nanofluids', and 'trihybrid nanofluids' are all terms used to describe these fluids. Since this research was motivated by previous studies on ternary hybrid nanofluid and MHD flow into a stretching/shrinking cylinder with mass suction and either Joule or ohmic heating, the current investigation is theoretical. Due to the substantial literature on copper nanoparticles, it has been selected as an example of ternary hybrid nanofluid, and we propose to investigate the impact of the combination of copper nanoparticles (Cu), iron oxide(Fe_3O_4), and silicon dioxide (SiO_2) with polymer as the base fluid. Additionally, the model exhibits the innovative and adaptable characteristics of mass suction, magnetic field, and ohmic heating, among others. Also, the form properties of the nanoparticles are examined. The shooting method is used to do numerical calculations once the modelling and simulations have been completed. The characteristics, form structures, and thermal traits of nanoparticles are graphically and tabulated analyzed in a comprehensive manner. This may be useful in future studies to increase heat transfer efficiency in modern industrial environments. All the authors are certain that the current study has not been previously reported in other publications.

2. Description of the problem

The current work considers steady, two-dimensional, magnetic field stagnation point flow of incompressible ternary hybrid nanofluid formed by suspended Cu, Fe_3O_4 and TiO_2 in polymer as base fluid. Grasp Fig. 1 for an illustration of a flow innovator. In this case, the permeable stretching/shrinking cylinder is defined by radius a, mass suction u_w, and joule heating is calculated around the cylindrical polar coordinates (z, r), where z is the axial and r is the radial length synchronize along the flow direction, correspondingly. It is also presumed that the mass transfer velocity is u_w, where $u_w > 0$ denotes suction and the magnetic field strength is denoted by B_0, correspondingly. The flow is presumed to be symmetric around the $z = 0$ plane and axisymmetric about the $z-$axis, with the stagnation line is at $z = 0$ and $r = a$. The surface velocity of the cylinder is given as $v_w(z) = 2bz$, where the static cylinder is indicated by $b = 0$, whereas the cylinder is stretched or shrunk when$b > 0$ or$b < 0$, correspondingly. In the

meantime, the free stream velocity is taken as $\mathrm{w_e(z)} = 2cz$, where$c > 0$. Moreover, the surface temperature T_w and the ambient temperature T_∞ are constant, where $T_w > T_\infty$. The equations can be simplified by reducing their similarity by using the predetermined surface temperature. While analyzing ternary nanofluids, several assumptions are made about the physical model. In addition, it is assumed that the nanoparticle's shape is cylindrical and that its size is homogeneous, while agglomeration is neglected since the ternary hybrid nanofluid is created as a stable composite and so does not agglomerate. Therefore, the equations that govern the ternary hybrid nanofluid flow are [28], [34]:

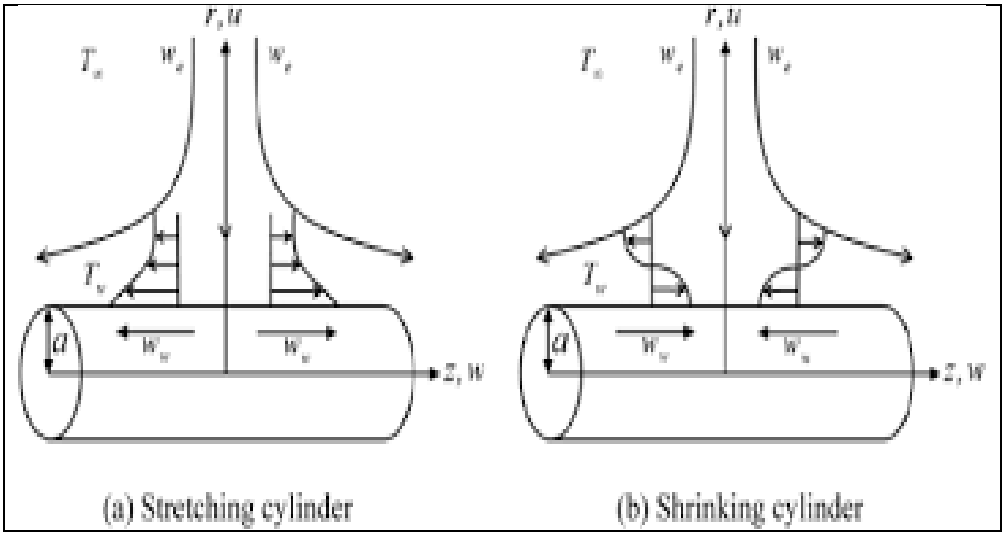

Figure 1 Flow configuration model of cylinder

$$\frac{\partial(rw)}{\partial z} + \frac{\partial(ru)}{\partial r} = 0, \tag{1}$$

$$w\frac{\partial \mathrm{w}}{\partial \mathrm{z}} + u\frac{\partial \mathrm{w}}{\partial r} = w_e\frac{dw_e}{dz} + \frac{\mu_{mnf}}{\rho_{mnf}}\left(\frac{\partial^2 w}{\partial r^2} + \frac{1}{r}\frac{\partial \mathrm{w}}{\partial \mathrm{r}}\right) - \frac{\sigma_{mnf}}{\rho_{mnf}}B^2{}_0(u - u_e), \tag{2}$$

$$w\frac{\partial \mathrm{T}}{\partial \mathrm{z}} + u\frac{\partial \mathrm{T}}{\partial r} = \frac{k_{mnf}}{(\rho C_p)_{mnf}}\left(\frac{\partial^2 T}{\partial r^2} + \frac{1}{r}\frac{\partial \mathrm{T}}{\partial \mathrm{r}}\right) + \frac{\sigma_{mnf}}{\rho_{mnf}}B^2{}_0u^2. \tag{3}$$

u and w symbolizes the velocity component beside the r-and z-directions respectively. Next, the boundary conditions are:

$$u = u_w, w = w_w, T = T_w \text{ at } r = a,$$

$$w \to w_e, T \to T_\infty \text{ as } r \to \infty. \tag{4}$$

Temperature of the ternary hybrid nanofluid is T, the dynamic viscosity is μ_{mnf}, the density is ρ_{mnf}, the thermal conductivity is k_{mnf} and the heat capacity $\left(\rho C_p\right)_{mnf}$.

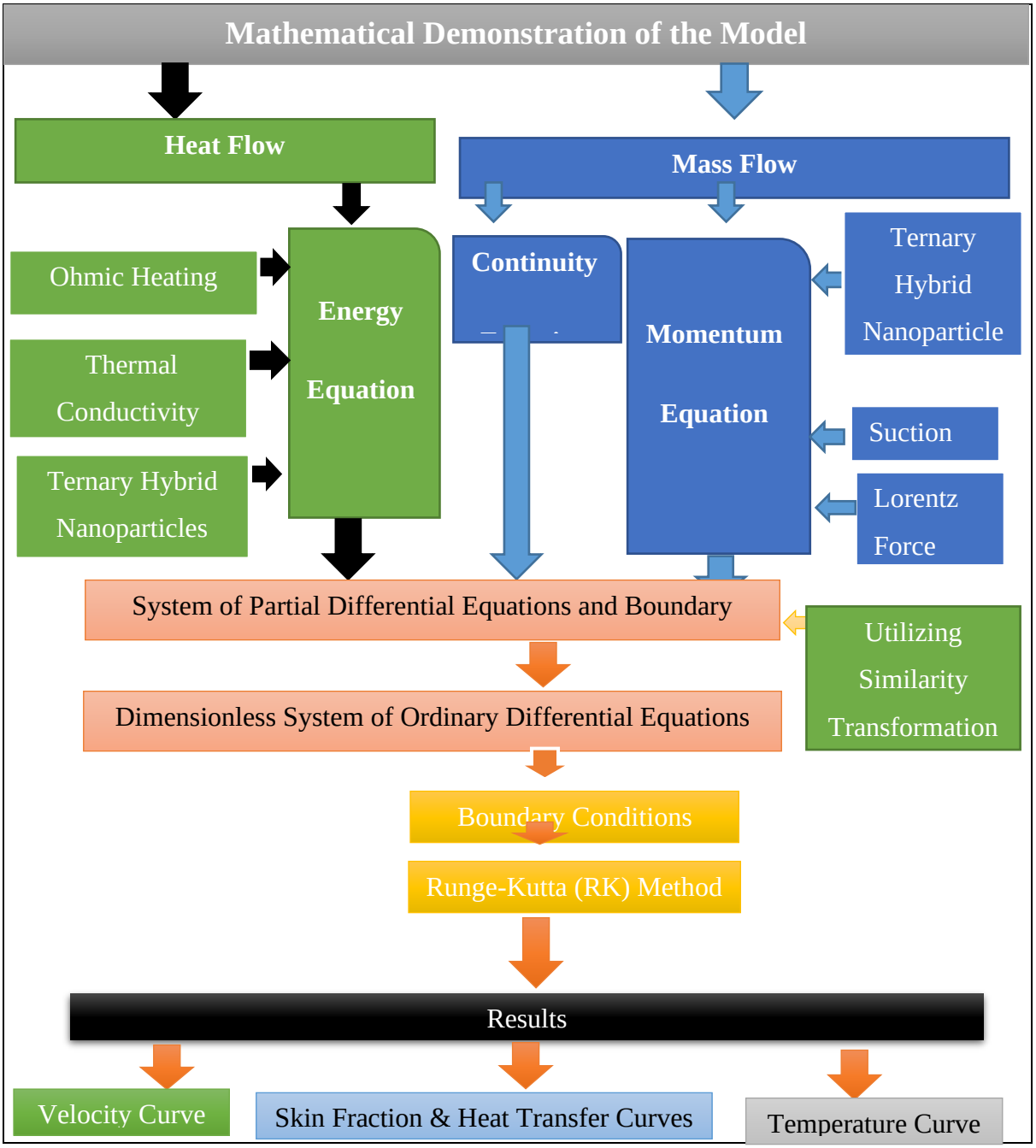

Figure 2 Model Simulation

The Table 1 provides several thermophysical properties for copper, iron oxide, silicon dioxide and polymer as the base fluid. Tables [2-4] provides a mathematical representation of the thermal characteristics of nanofluid, hybrid nanofluid and ternary hybrid nanofluid. Furthermore, Table 5 shows the numerical values for different form factors based on the shape characteristics m. In Table 1 $\phi_1$is volume fraction of Cu, ϕ_2 is volume fraction ofFe_3O_4 and ϕ_3 is volume fraction of SiO_2 nanoparticles. Subscripts $s1, s2$, and$s3$ stands for denoting the properties of Cu, Fe_3O_4, and SiO_2 nanoparticles.

Table 1 Numerical values of polymer base and ternary hybrid nanoparticles [35]–[37]

Properties	$Cu\ (\phi_1)$	$Fe_3O_4(\phi_2)$	$SiO_2(\phi_3)$	$polymer$
$\rho\ (kg/m^3)$	8933	5180	2650	1060
$Cp\ (J/kgK)$	385	670	730	3770
$k\ (W/mK)$	401	9.7	1.5	0.429
$\sigma(\Omega m)^{-1}$	5.96×10^7	2.5×10^{-4}	1.0×10^{-18}	4.3×10^{-5}
Pr				6.2

Table 2 Thermo-physical property of Nanofluid [28]

Density	$\boldsymbol{\rho_{nf} = (1-\phi_1)\rho_f + \phi\rho_{s1}}$
Viscosity	$\mu_{nf} = \frac{\mu_f}{(1-\phi_1)^{2.5}}$
Heat capacity	$(\rho C_p)_{nf} = (1-\phi_1)(\rho C_p)_f + \phi(\rho C_p)_{s1}$
Thermal conductivity	$\frac{k_{nf}}{k_f} = \frac{k_{s1} + 2k_f - 2\phi_1(k_f - k_{s1})}{k_{s1} + 2k_f + \phi_1(k_f - k_{s1})}$

Table 3 Thermo-physical property of Hybrid nanofluid [28]

Density	$\boldsymbol{\rho_{hnf} = (1-\phi_2)\left[(1-\phi_1)\rho_f + \phi_1\rho_{s1}\right] + \phi_2\rho_{s2}}$
Viscosity	$\mu_{nf} = \frac{\mu_f}{(1-\phi_1)^{2.5}(1-\phi_2)^{2.5}}$
Heat capacity	$(\rho C_p)_{hnf} = (1-\phi_2)\left[(1-\phi_1)(\rho C_p)_f + \phi_1(\rho C_p)_{s1}\right] + \phi_2(\rho C_p)_{s2}$
Thermal conductivity	$\frac{k_{hnf}}{k_{nf}} = \frac{k_{s2}+2k_{nf}-2\phi_2(k_{nf}-k_{s2})}{k_{s2}+2k_{nf}+\phi_2(k_{nf}-k_{s2})}$, where $\frac{k_{nf}}{k_f} = \frac{k_{s1} + 2k_f - 2\phi_1(k_f - k_{s1})}{k_{s1} + 2k_f + \phi_1(k_f - k_{s1})}$

Table 4 Thermal property of Ternary hybrid nanofluid [38].

Properties	Ternary Hybrid nanofluid
Density	$\rho_{mnf} = (1-\phi_3)\left\{(1-\phi_2)\left[(1-\phi_1)_{\rho_f} + \phi_1\rho_{s1}\right] + \phi_2\rho_{s2}\right\} + \phi_3\rho_{s3}$
Dynamic Viscosity	$\mu_{mnf} = \frac{\mu_f}{(1-\phi_3)^{2.5}(1-\phi_2)^{2.5}(1-\phi_1)^{2.5}}$
Thermal Conductivity	$\frac{k_{mnf}}{k_{hnf}} = \frac{k_{s3}+(m-1)k_{hnf}-(m-1)\phi_3(k_{hnf}-k_{s3})}{k_{s3}+(m-1)k_{hnf}+\phi_3(k_{hnf}-k_{s3})}$,Where $\frac{k_{hnf}}{k_{nf}} = \frac{k_{s2} + (m-1)k_{nf} - (m-1)\phi_2(k_{nf} - k_{s2})}{k_{s2} + (m-1)k_{nf} + \phi_2(k_{nf} - k_{s2})}$,

	and $\frac{k_{nf}}{k_f} = \frac{k_{s1}+(m-1)k_f-(m-1)\phi_1(k_f-k_{s1})}{k_{s1}+(m-1)k_f+\phi_1(k_f-k_{s1})}$.
Heat Capacity	$(\rho C_p)_{mnf} = (1-\phi_3)\left\{(1-\phi_2)\left[(1-\phi_1)(\rho C_p)_f + \phi_1(\rho C_p)_{s1}\right] + \phi_2(\rho C_p)_{s2}\right\} + \phi_3(\rho C_p)_{s3}$

Table 5 Distinct nanoparticles have different form factors [38].

Forms of nanoparticles	Numerical values
Bricks	3.7
Platelets	5.7
Cylinders	4.9
Blades	8.6

As a consequence of following, [28] a similarity transformation is now suggested to arrive at similarity solutions:

$$u = \frac{acf(\eta)}{\sqrt{\eta}}, w = 2czf'(\eta), \theta(\eta) = \frac{T-T_\infty}{T_w-T_\infty}, \eta = \left(\frac{r}{a}\right)^2. \quad (5)$$

Where prime indicates differentiation in relation to η. The following ordinary differential equations are drawn by including (1), (2), (3) and (5) in the steady-state equations.

$$\frac{\mu_{mnf}}{\rho_{mnf}}(\eta f''' + f'') + Re\left(ff'' - f'^2 + 1\right) - M^2\frac{\sigma_{mnf}}{\rho_{mnf}}(f'-1) = 0, \quad (6)$$

$$\frac{1}{Pr}\frac{k_{mnf}}{(\rho C_p)_{mnf}}(\eta\theta'' + \theta') + Ref\theta' + EcM^2\frac{\sigma_{mnf}}{\rho_{mnf}}(f')^2 = 0. \quad (7)$$

Transformation of boundary conditions (4) into

$$f(1) = S, f'(1) = \delta, \theta(1) = 1,$$
$$f'(\eta) \to 1, \theta(\eta) \to 0, \ as\ \eta \to \infty. \quad (8)$$

In the preceding equations, $\mathrm{Re} = \frac{ca^2}{2v_f}$ signifies the Reynold number and $Pr = \frac{\mu_f(Cp_f)_f}{k_f}$ denotes the Prandtl number. $S = -\frac{u_w}{\sqrt{av_f}}$ represents the steady mass flux parameter($S > 0$ for suction. By $\delta = \frac{b}{c}$, we mean the stretch/shrink parameter, where $\delta > 0$ indicates a sheet that is stretched and $\delta < 0$ represents a sheet that is shrinking. $M = \frac{\sigma_f {B^2}_0}{a\rho_f}$ denotes magnetic parameter. $Ec = \frac{u^2\rho_f}{(T_f-T_\infty)(\rho C_p)_{nf}} = \frac{a^2\rho_f}{(\rho C_p)_{nf}}$ is Eckert number. The friction coefficients C_f in addition to local Nusselt number Nu, are of particular importance in this investigation.

$$C_f = \frac{2}{\rho_f w_e{}^2}\mu_{mnf}\left(\frac{\partial w}{\partial r}\right)_{r=a}, Nu = -\frac{a}{k_f(T_w - T_\infty)}k_{mnf}\left(\frac{\partial T}{\partial r}\right)_{r=a}. \quad (9)$$

Equations (5) and (9) yield the following:

$$\left(\frac{Re_z}{a}\right)C_f = \frac{\mu_{mnf}}{\mu_f}f''(1),\ Nu = -\frac{2K_{mnf}}{k_f}\theta''(1), \quad (10)$$

3. Numerical Procedure for Solution

The coupled nonlinear ordinary differential equations 6-7 and related boundary conditions 8 are very complicated and nonlinear in nature. It would be better if a numerical scheme is applied to deal with these equations. Ternary hybrid nanofluid flow paths for various physical variables are captured by combining RK-IV and shooting methods. A few transformations are needed depending on the sequence in which the self-similar momentum and energy equations 6-7 together with boundary domains contained in equations 8, are used to start the process.

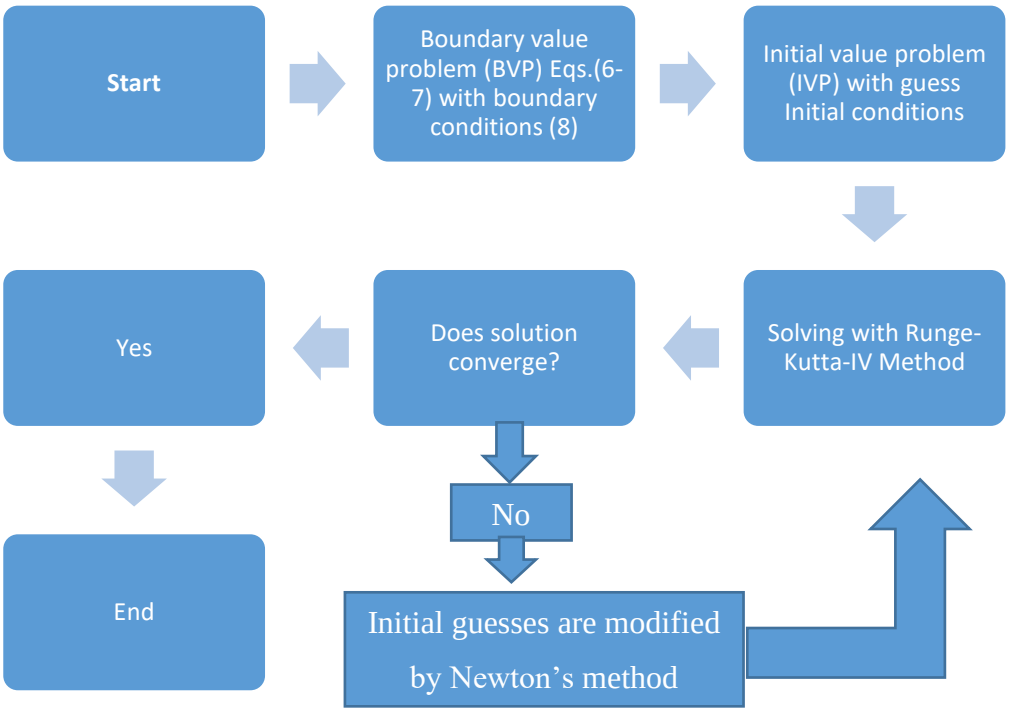

Figure 3 Schematic diagram for shooting method

These changes reduced the model to a first-order initial value issue, which can then be solved as follows:

$$Z_1 = f, Z_2 = f', Z_3 = f'', Z_4 = \theta, Z_5 = \theta' \quad (11)$$

using the equation (11),

$$Z'_1 = f', Z'_2 = f'', Z'_3 = f''', Z'_4 = \theta', Z'_6 = \theta'', \quad (12)$$

Using equation (11, 12) in (6-8) and after rearranging equations, we get the following:

$$Z'_3 = -\left(\frac{\rho_{mnf}/\rho_f}{\mu_{mnf}/\mu_f}\right)\frac{1}{\eta}\left[Z_3 + Re\left(Z_1 Z_3 - {Z_2}^2 + 1\right) - M^2\,\frac{\sigma_{mnf}}{\rho_{mnf}}(Z_2 - 1)\right], \quad (13)$$

$$Z'_6 = -Pr\,\frac{(\rho C_p)_{mnf}}{k_{mnf}}\frac{1}{\eta}\left[Z_5 + ReZ_1 Z_5 + EcM^2\,\frac{\sigma_{mnf}}{\rho_{mnf}}(Z_2)^2\right], \quad (14)$$

$$Z_1(1) = S, Z_2(1) = \delta, Z_4(1) = 1, Z_3 \to 1, Z_5 \to 0 \quad (15)$$

To solve the resulting initial value issue, we must include the values from equations 13-14 in equations 6-8, respectively. To get numerical solutions of (6-8), a highly capable computational software package called Mathematica 10 is utilized. It has a unique property that it classifies the governing system and applies the most suitable numerical procedure to provide accurate solutions for the system.

4. Results and Discussion

The shooting technique with RK-IV is used to solve Equations (6) to (8) in the computational software Mathematica which we discussed in previous section, figures and tables are used to illustrate the numerical findings. The boundary layer thickness $\eta_\infty = 20.$ and $Pr = 6.2$ is fixed except for evaluation as seen in the tables and figures, control characteristics are varying. These values are determined by whether the far-field boundary requirements are met (8). Since nano, hybrid and $Cu - Fe_3O_4 - SiO_2/\text{polymer}$ ternary hybrid nanofluid is supported in this current work, a different set of ϕ values fraction is limited in between $0.005 \le \phi \le 0.02$. Other parameters, such as $2.0 \le S \le 2.5$ (suction), $-1.0 \le \delta \le 1$ (stretching/shrinking), $10^{-6} \le M \le 5 * 10^{-6}$ (magnetic parameter), $0.0 \le Re \le 1.0$,(Reynold number) and $0.1 \le Ec \le 0.6$(Eckret number) are selected grounded on the primary citations and the possibilities of results.

In Fig. 1, the flow of a ternary hybrid nanofluid is shown as a physical model. Model simulation is represented by a flow chart in Fig. 2. Consequences for velocity, temperature, skin friction, and local heat transfer curves are presented in Figs. 4-23, which provide a comprehensive picture of the present condition for stretching and shrinking surface. In the coming section, graphical comparison of nanofluid, hybrid nanofluid and ($Cu - Fe_3O_4 - SiO_2/\text{polymer}$) ternary hybrid nanofluids are discussed.

4.1 Velocity $f'(\eta)$ and Temperature $\theta(\eta)$ Curves for Stretching and Shrinking Cylindrical Surface

In this subsection we discussed in detail the impacts of different parameters such as: volume fraction(ϕ_1, ϕ_2, ϕ_3), magnetic field M, suction S, stretching/shrinking δ, Reynold number Re and Eckert number EC on the axial velocity $f'(\eta)$ and temperature $\theta(\eta)$ curves of nanofluid, hybrid nanofluid and ternary hybrid nanofluid. For nanofluid $(Cu/\text{polymer})$ case, we consider ϕ_1, for hybrid nanofluid$(Cu - Fe_3O_4/\text{polymer})$, we consider $\phi_1$and ϕ_2, while for ternary hybrid nanofluid$(Cu - Fe_3O_4 - SiO_2/\text{polymer})$, we take$\phi_1$,$\phi_2$ andϕ_3.

As the cylinder shrinks, the velocity and temperature curves are affected by the volume fractions of copper ϕ_1, iron oxide ϕ_2, and silicon dioxide ϕ_3, as seen in Figures 4 and 5. There is greater space for improved heat conduction in nanofluids with higher volume fractions of nanoparticles, which are found in metal and metal oxide, in hybrid nanofluid, and in ternary hybrid nanofluids. Thus, the nanofluid, hybrid nanofluid, and ternary nanofluid all become hotter as can be shown in Figure 5. This implies that the device's heat absorption is boosted, ensuring an optimal temperature and a long service life for the appliance. A heat conductor with a photocatalytic nature like metal and metal oxide nanoparticles is more suited to use as a nanofluid or hybrid nanofluid or ternary hybrid nanofluid, since they are better at conducting heat than other types of nanoparticles. Nanofluid, hybrid nanofluid, and ternary hybrid nanofluid are all made more stable by their chemical inertness. As previously noted, reducing air pollution by employing this mixture as a coolant in automobiles is possible. Nanofluid, hybrid nanofluid, and ternary hybrid nanofluid lose density and flow more readily due to the increased heat conductivity of these nanoparticles. The fluid's flow velocity increases as a result of these less dense nanoparticles pulling it in the same direction as the fluid itself. Clearly, one can see that ternary hybrid nanofluid has higher temperature profiles ac compared to nano and hybrid nanofluid owing to the existence of more nanoparticles.

Using the shrinking scenario as an example, Figures 6 and 7 show how the magnetic field M affects the velocity and temperature curves of the nanofluid, hybrid nanofluid, and tri-hybrid nanofluid. A force termed the Lorentz force opposes fluid flow when there is a magnetic field present. This force's magnitude is directly related to the magnitude of M. When a result, as M rises, the Lorentz force becomes stronger. With larger levels of M, the momentum of the fluid flow decreases as a result of this increased resistance. When flow velocity is reduced, more heat may be conducted by nanoparticles, resulting in higher temperatures.

Figures 8-9 illustrates the consequence of suction constraint S on velocity curve $f'(\eta)$ and temperature curve $\theta(\eta)$ for shrinking cylinder case of the nanofluid, hybrid nanofluid and ternary hybrid nanofluid flow. In Figs.8 velocity curve increase with the expanding values of the suction S. This is because the density has grown due to the addition of more particles. By lowering the thickness of the momentum barrier layer, suction improves the flow of the stretched and shrinking surface. Temperature variations with suction parameter S are shown in Fig. 9 as a function of temperature. Temperature falls when the parameter S increases in value. suction cools the boundary layer flow, which means that suction is also used in many industrial processes, as well as nuclear energy and MHD power plants.

Nanofluid, hybrid nanofluid and ternary hybrid nanofluid velocity and temperature curves for stretching cylinder case $\delta > 0$ are shown in Figure 10 and 11. When the velocity ratio parameter is increased, fluid velocity drops, but the temperature curve shows the opposite. It has a physical impact in that growing the rate of δ findings in a diminution in the thickness of the momentum boundary layers as time goes on. The thermal boundary layer thickens as a sheet shrinks, which is also important to notice.

The effect of Re on$f'(\eta)$ and $\theta(\eta)$ when$\phi_1 = \phi_2 = \phi_3 = 0.005, \delta = -0.5, S = 2.0, M = 10^{-6}, m = 4.9$ and$Pr = 6.2$ for nanofluid, hybrid nanofluid and ternary hybrid nanofluid for shrinking cylinder case are exhibited in Figs. 12 and 13. Magnetic parameter supposedly reduces velocity due to Lorentz force, however in this case, the velocity rises due to the Lorentz force. When the Reynolds number Re is increased, the velocity$f'(\eta)$ rises, and as a consequence, the temperature $\theta(\eta)$ drops after the thermal diffusion is overcome, as seen in the graph. A shrinking cylinder nanofluid, a hybrid nanofluid, and a ternary hybrid nanofluid are all shown in Figure 14 to show the effect of Ec on the temperature curve $\theta(\eta)$. This value represents the rate at which heat is dissipated across the system.

The temperature curve $\theta(\eta)$ of nanofluid, hybrid nanofluid and ternary hybrid nanofluids are shown in Fig. 14 under the impact of Eckert number Ec. When the Eckert number is raised along the stretching/shrinking cylinder, we see a spike in the temperature distribution curve with $Ec = 0.005, 0.1, 0.15, 0.2,$ $S = 2.0, \delta = -0.5, Re = 0.5, M = 10^{-6}, m = 4.9, \phi_1 = \phi_2 = \phi_3 = 0.005$ and $Pr = 6.2$. Ec is obtained mostly from the relationship between advective transport and heat dissipation potential. An increase in Ec parameter values increases $\theta(\eta)$ and the thickness of the associated layer. The boundary layer at the surface of the decreasing cylinder may induce a thermal reversal mechanism that causes this occurrence. The higher the temperature of the nanofluid, hybrid nanofluid, or ternary hybrid nanofluid, the more

kinetic energy is converted to heat energy. A rise in the Eckert number, which measures the kinetic energy and enthalpy ratio, causes an increase in the thermal state of the nanofluid, a hybrid nanofluid, and a ternary hybrid nanofluid, as shown in the temperature distribution profile. This causes the thermal boundary layer to rise, which reduces heat transfer, as shown in the temperature distribution.

It can be shown from these figures that ternary hybrid nanoparticles have a considerable effect on thermal performance when compared to other nanoparticles. It is ternary hybrid nanoparticles that create the greatest amount of thermal energy, rather than hybrid nanoparticles and simple nanoparticles.

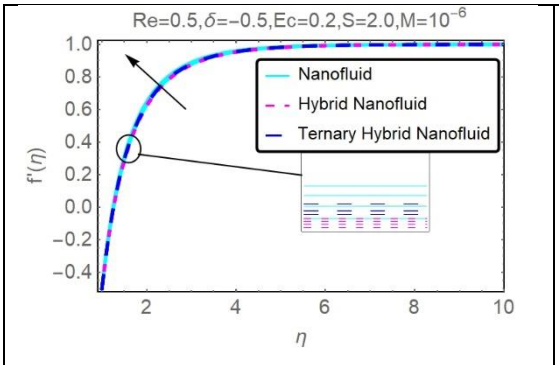

Figure 4 Change in $f'(\eta)$ with $(\phi_1, \phi_2, \phi_3) = 0.005,0.01,0.015,0.02$.

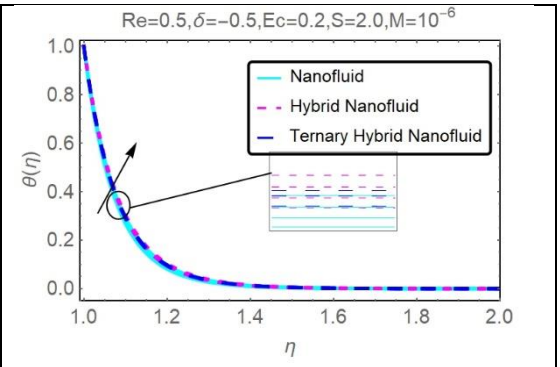

Figure 5 Variation in $\theta(\eta)$ with $(\phi_1, \phi_2, \phi_3) = 0.005,0.01,0.015,0.02$.

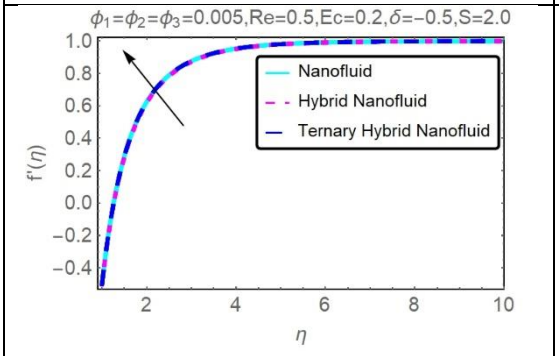

Figure 6 Variation in $f'(\eta)$ with $M = 10^{-6}, 2 * 10^{-6}, 3 * 10^{-6}, 4 * 10^{-6}$.

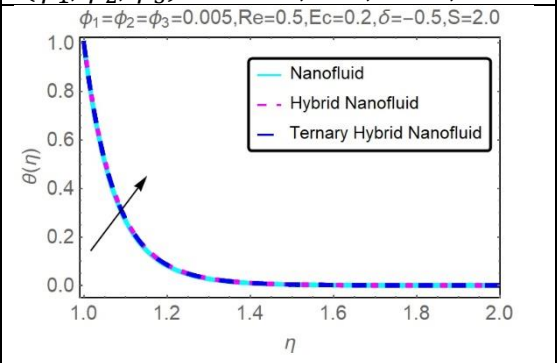

Figure 7 Variation in $\theta(\eta)$ with $M = 10^{-6}, 2 * 10^{-6}, 3 * 10^{-6}, 4 * 10^{-6}$.

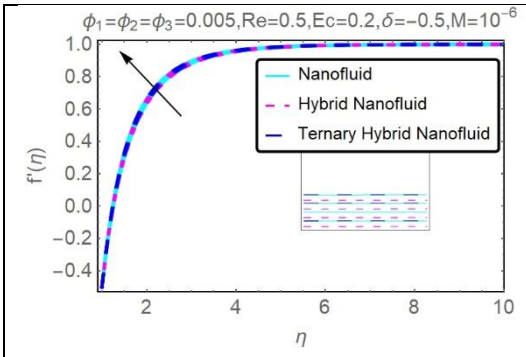

Figure 8 Variation in $f'(\eta)$ with $S =$ 2.1,2.2,2.3,2.4.

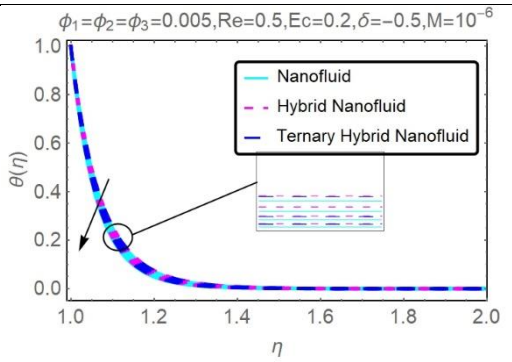

Figure 9 Variation in $\theta(\eta)$ with $S =$ 2.1,2.2,2.3,2.4.

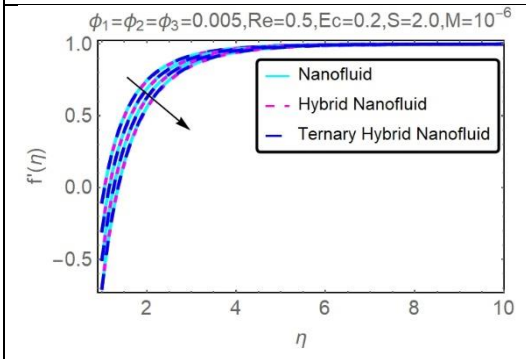

Figure 10 Variation in $f'(\eta)$ with $\delta =$ 0.2,0.4,0.6,0.8.

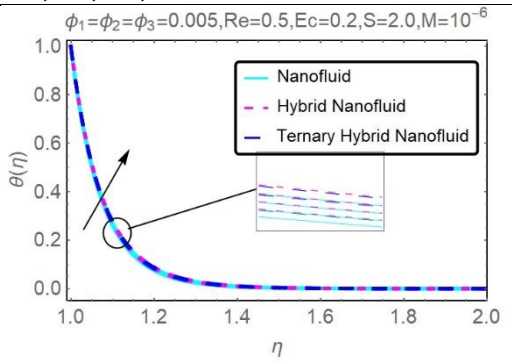

Figure 11 Variation in $\theta(\eta)$ with $\delta =$ 0.2,0.4,0.6,0.8.

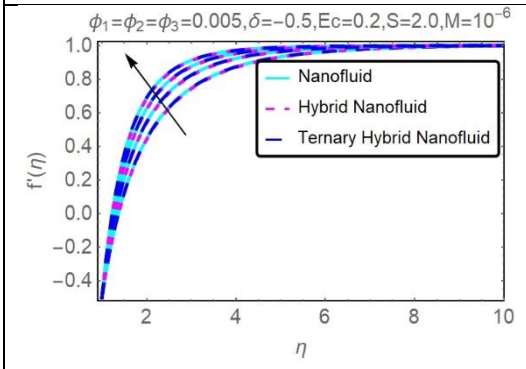

Figure 12 Variation in $f'(\eta)$ with $Re =$ 0.3,0.4,0.5,0.6.

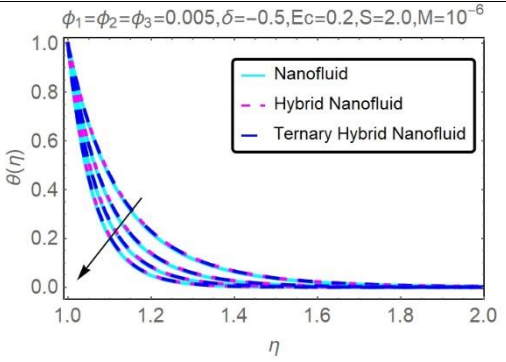

Figure 13 Variation in $\theta(\eta)$ with $Re =$ 0.3,0.4,0.5,0.6.

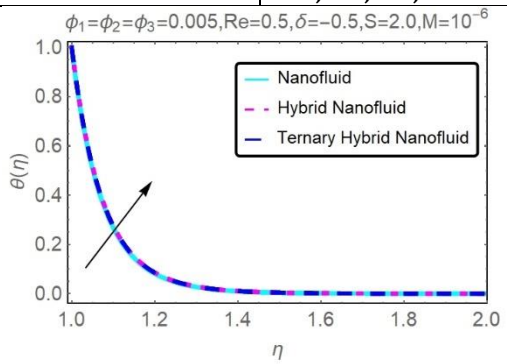

Figure 14 Variation in $\theta(\eta)$ with $Ec =$ 0.2,0.3,0.4,0.5.

4.3 Skin Friction and Heat Transfer

This subsection highlights impression of different parameters against physical measures such as skin friction and local heat transfer rate. The local heat transfer rate Nu and skin friction $\left(\frac{Re_z}{a}\right)C_f$ are critical industrial parameters. Due to industrial uses, the importance of these numbers cannot be disputed. Skin friction coefficients$\left(\frac{Re_z}{a}\right)C_f$and local heat transfer rate Nu vary according to changes in parameters.

Figures 15 and 16 illustrate the increasing effect of stretching and shrinking parameters δ towards volume fraction (ϕ_1, ϕ_2, ϕ_3) on the $\left(\frac{Re_z}{a}\right)C_f$ and local heat transfer rate $Nu$of nano, hybrid, and ternary hybrid nanofluid when $S = 2.0, M = 10^{-6}, m = 4.9, Re = 0.5, Ec = 0.2$ and $Pr = 6.2$. The positive values of δ provides stretching and negative values of δ provides shrinking of the cylinder. It is demonstrated in Figs.15 and 16 by various values of δ with (ϕ_1, ϕ_2, ϕ_3)decreasing the $\left(\frac{Re_z}{a}\right)C_f$ and increases Nu. Specifically, larger concentrations of nanoparticles create more kinetic energy than lower concentrations, which increases the heat transmission of fluid particles by increasing their kinetic energy.

Figures 17 and 18 show the impact of S with (ϕ_1, ϕ_2, ϕ_3) against skin friction coefficient $\left(\frac{Re_z}{a}\right)C_f$ and (Nu) of nano, hybrid, and ternary hybrid nanofluid for shrinking cylinder case. For all values of$S = 2.0, 2.1, 2.2, 2.3, 2.4, 2.5$, when $\delta = -0.5, M = 10^{-6}, m = 4.9, Re = 0.5, Ec = 0.2$ and $Pr = 6.2$. Solutions for extending surfaces, flows may be established without the use of suction. In order to improve $\left(\frac{Re_z}{a}\right)C_f$ and (Nu), suction is necessary. Suction, on the other hand, is useful in the enhancement of both the skin fraction and the local heat transfer rate. When hot fluid particles are suctioned toward a surface, they move faster and more efficiently, increasing heat transfer.

The effect of magnetic field parameter M towards (ϕ_1, ϕ_2, ϕ_3) on the $\left(\frac{Re_z}{a}\right)C_f$ and (Nu) can be illustrated from Figure 19 and 20 for shrinking cylinder of nanofluid, hybrid nanofluid and ternary hybrid nanofluid. For all values of$M = 10^{-6}, 1 * 10^{-6}, 2 * 10^{-6}, 3 * 10^{-6}, 4 * 10^{-6}, 5 * 10^{-6}$, when $\delta = -0.5, S = 2.0, m = 4.9, Re = 0.5, Ec = 0.2$ and $Pr = 6.2$. It is clear from these results that raising M, the $\left(\frac{Re_z}{a}\right)C_f$ and (Nu) boosts. For this reason, an additional amount of energy is transferred into the boundary layer as the Lorentz force grows over time.

Variations in the skin friction coefficient $\left(\frac{Re_z}{a}\right)C_f$ and the Nusselt number Nu may be seen in Figures 21 and 22 versus (ϕ_1, ϕ_2, ϕ_3). Intended for all estimates of $Re = 0.2, 0.4, 0.6, 0.8, 1.0$, when $\delta = -0.5, M = 10^{-6}, S = 2.0, m = 4.9, Ec = 0.2$ and $Pr = 6.2$. An increase in Re has a comparable impact as a decrease in nanoparticles, hybrid nanoparticles and ternary hybrid nanoparticles on the skin friction $\left(\frac{Re_z}{a}\right)C_f$. Reynolds number Re is a physical indicator of the relative importance of the inertial forces relative to the viscous forces. For rising Reynolds numbers, the skin friction coefficient (surface shear-stress) increases. The Nusselt number Nu is boosted by the rise of Re. In addition, it has been observed that the increase is more prominent in the stretching situation.

Figure 23 depict the variation of the Nusselt number Nu against (ϕ_1, ϕ_2, ϕ_3) For all values of $Ec = 0.1, 0.2, 0.3, 0.4, 05,$ when $\delta = -0.5, M = 10^{-6}, S = 2.0, m = 4.9, Re = 0.5$ and $Pr = 6.2$ for shrinking cylinder of nanofluid, hybrid nanofluid and ternary hybrid nanofluid. As expected, the coefficient of heat transfer reduced with increment of Eckert number.

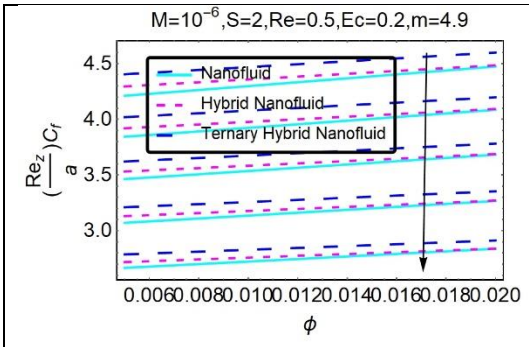

Figure 15 Variation in $\left(\frac{Re_z}{a}\right)C_f$ in contract to δ towards (ϕ_1, ϕ_2, ϕ_3).

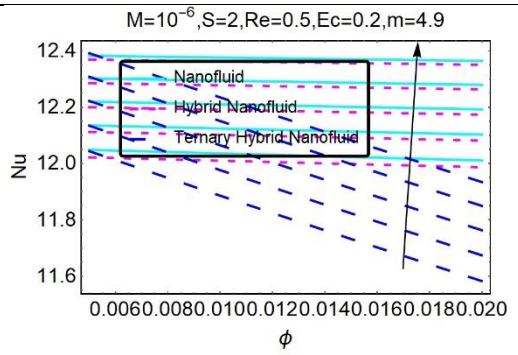

Figure 16 Variation in Nu in contract to δ towards (ϕ_1, ϕ_2, ϕ_3).

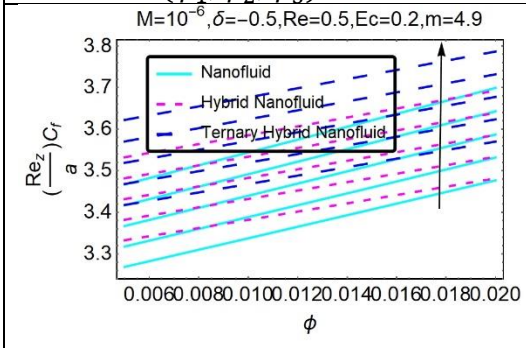

Figure 17 Variation in $\left(\frac{Re_z}{a}\right)C_f$ in contract to S towards (ϕ_1, ϕ_2, ϕ_3)

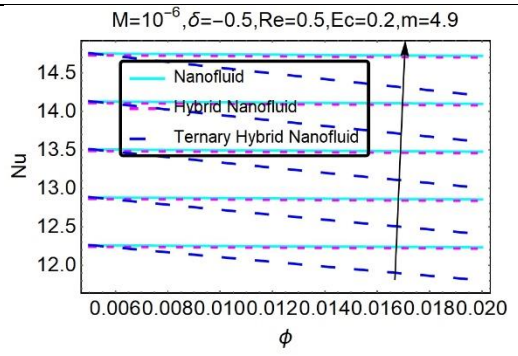

Figure 18 Variation in Nuin contract to S towards (ϕ_1, ϕ_2, ϕ_3)

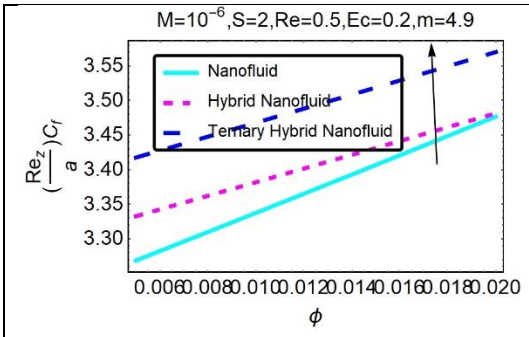

Figure 19 Variation in $\left(\frac{Re_z}{a}\right) C_f$ in contract to M towards (ϕ_1, ϕ_2, ϕ_3).

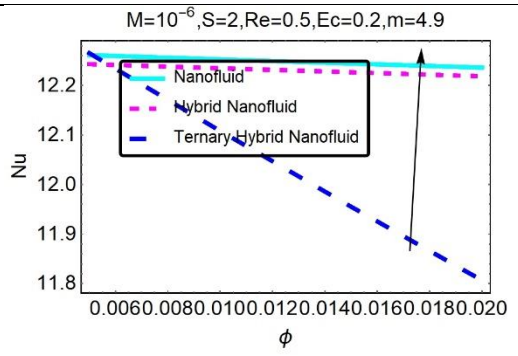

Figure 20 Variation in Nuin contract to Mtowards (ϕ_1, ϕ_2, ϕ_3)

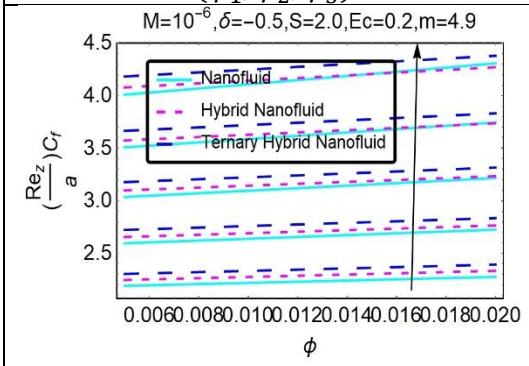

Figure 21 Variation in$\left(\frac{Re_z}{a}\right) C_f$ in contract to Re towards (ϕ_1, ϕ_2, ϕ_3)

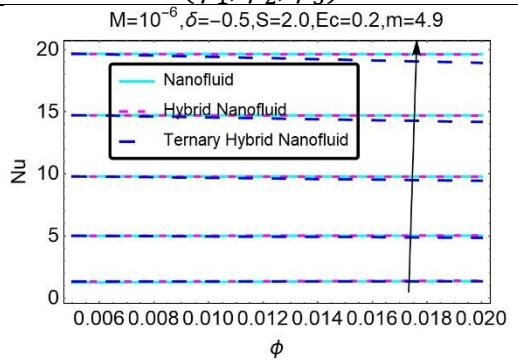

Figure 22 Variation in Nu in contract to Re towards (ϕ_1, ϕ_2, ϕ_3)

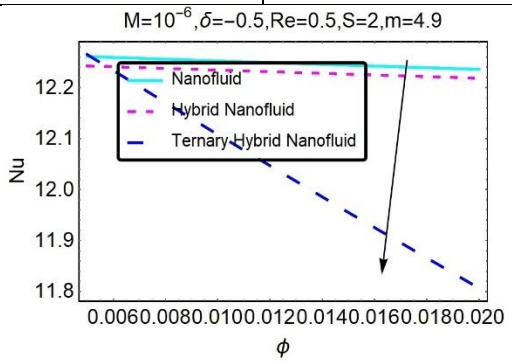

Figure 23 Variation in Nuin contract to Ec towards (ϕ_1, ϕ_2, ϕ_3)

4.4 Table Discussion

The comparisons of result in Table 6 are presented to validate the numerical procedure of the current study with the numerical results from [28] for a different value of Re for regular fluid when $\phi_1 = \phi_2 = \phi_3 = \delta = M = S = 0$. The previous studies by [28] tackled the hybrid nanofluid fluid problem, while the present study implemented the ternary hybrid nanofluid. Further, [28] used bvpc4c in MATLAB while this study applied the shooting with Runge-Kutta-IV procedure in the Mathematica. These findings are found to be in accord with the

previously found; thus, this gives us confidence that the computational structure to scrutinize the ternary hybrid nanofluid flow behaviors and heat transfer in this study can be employed with significant assurance. The arrangement of suitable single/hybrid and ternary nanofluids is the most important factor in defining nanofluid flow behavior and heat transfer efficiency.

Table 6 Estimates of$f''(1)$ and $-2\theta'(1)$ produces results for specific values of Re

Re	Present	Waini [28]	Present	Waini [28]
	$f''(1)$	$f''(1)$	$-2\theta'(1)$	$-2\theta'(1)$
0.2	0.95206	0.786042	1.61109	1.508635
1	1.50033	1.484183	2.80286	2.793424
10	4.16412	4.162920	8.2772	7.701472

5. Conclusion:

The major result of the current research is that the rate of heat transfer may be increased. Polymer based nanofluid(Cu/polymer), hybrid nanofluid($Cu - Fe_3O_4$/polymer), and ternary hybrid nanofluid($Cu - Fe_3O_4 - SiO_2$/polymer) nanoparticles with cylindrical shape features has been utilized to flow across a permeable stretching/shrinking cylindrical surface with mass suction, Lorentz force and ohmic heating to find a two-dimensional Stagnation point. The thermophysical characteristics have been taken from the available literature and used in this experiment. To increase the heat transmission rate, it is necessary to consider the suction with nanoparticles volume fraction. Partial differential equations (PDEs) were used to represent fundamental governance equations, which were then converted into a set of ordinary differential equations (ODEs) that could be used for transformations and optimizations. The best strategy shooting techniques with Runge Kutta-IV in computational software Mathematica was used to find solution. Graphs depict the impact of different variables on velocity and temperature curves. Graphical representations are also used to show the main properties such as skin friction coefficient and local heat transfer rate. We can deduce the following from the data shown above:

- Both magnetic parameter M and nanoparticles concentration ϕ have similar effect on fluid velocity$f'(\eta)$ and temperature $\theta(\eta)$ curves of nanofluid(Cu/polymer), hybrid nanofluid ($Cu - Fe_3O_4$/polymer), and ternary hybrid nanofluid($Cu - Fe_3O_4 - SiO_2$/polymer) for shrinking cylinder.

- Variation in suction parameter increases velocity profiles and opposite behavior shown in temperature profile of nanofluid($Cu/\text{polymer}$), hybrid nanofluid($Cu-Fe_3O_4/\text{polymer}$), and ternary hybrid nanofluid($Cu-Fe_3O_4-SiO_2/\text{polymer}$) for shrinking cylinder.
- Both velocity field $f'(\eta)$ and temperature field $\theta(\eta)$ of nanofluid($Cu/\text{polymer}$), hybrid nanofluid($Cu-Fe_3O_4/\text{polymer}$), and ternary hybrid nanofluid($Cu-Fe_3O_4-SiO_2/\text{polymer}$) for shrinking cylinder have opposite impacts for larger values of Re.
- Both skin friction and heat transfer rat coefficients boosts due to the augmentation of both M and ϕ of nanofluid($Cu/\text{polymer}$), hybrid nanofluid($Cu-Fe_3O_4/\text{polymer}$), and ternary hybrid nanofluid($Cu-Fe_3O_4-SiO_2/\text{polymer}$) for shrinking cylinder case.
- The augmentation in nanoparticle volume concentration with stretching/shrinking increases both skin fraction and local heat transfer coefficients of nanofluid($Cu/\text{polymer}$), hybrid nanofluid($Cu-Fe_3O_4/\text{polymer}$), and ternary hybrid nanofluid($Cu-Fe_3O_4-SiO_2/\text{polymer}$) for this problem.
- An improvement in the suction constraint intensity can boost both the local skin fraction and heat transfer rate of the nanofluid($Cu/\text{polymer}$), hybrid nanofluid($Cu-Fe_3O_4/\text{polymer}$), and ternary hybrid nanofluid($Cu-Fe_3O_4-SiO_2/\text{polymer}$) for shrinking cylinder.
- As the stretching/shrinking parameter is increased, the velocity of the nanofluid($Cu/\text{polymer}$), hybrid nanofluid($Cu-Fe_3O_4/\text{polymer}$), and ternary hybrid nanofluid($Cu-Fe_3O_4-SiO_2/\text{polymer}$) decreased whereas temperature increased.
- Increasing values of Re with (ϕ_1, ϕ_2, ϕ_3) surge up both the curves for skin fraction and local heat transfer rate coefficients of the nanofluid($Cu/\text{polymer}$), hybrid nanofluid($Cu-Fe_3O_4/\text{polymer}$), and ternary hybrid nanofluid($Cu-Fe_3O_4-SiO_2/\text{polymer}$) for shrinking cylinder case.
- Increasing values of Ec with ϕ decline the curve of local heat transfer rate of the nanofluid($Cu/\text{polymer}$), hybrid nanofluid($Cu-Fe_3O_4/\text{polymer}$), and ternary hybrid nanofluid($Cu-Fe_3O_4-SiO_2/\text{polymer}$) for shrinking cylinder case.

To get the desired outcome, it is important to manage the amplitude of the essential factors.

References

[1] M.-W. Tian, S. Rostami, S. Aghakhani, A. S. Goldanlou, and C. Qi, "A techno-economic investigation of 2D and 3D configurations of fins and their effects on heat sink efficiency

of MHD hybrid nanofluid with slip and non-slip flow," *Int. J. Mech. Sci.*, vol. 189, p. 105975, 2021.

[2] I. Waini, A. Ishak, T. Groşan, and I. Pop, "Mixed convection of a hybrid nanofluid flow along a vertical surface embedded in a porous medium," *Int. Commun. Heat Mass Transf.*, vol. 114, p. 104565, 2020.

[3] D. D. Kumar and A. V. Arasu, "A comprehensive review of preparation, characterization, properties and stability of hybrid nanofluids," *Renew. Sustain. Energy Rev.*, vol. 81, pp. 1669–1689, 2018.

[4] T. R. Shah and H. M. Ali, "Applications of hybrid nanofluids in solar energy, practical limitations and challenges: a critical review," *Sol. energy*, vol. 183, pp. 173–203, 2019.

[5] N. A. C. Sidik, I. M. Adamu, M. M. Jamil, G. H. R. Kefayati, R. Mamat, and G. Najafi, "Recent progress on hybrid nanofluids in heat transfer applications: a comprehensive review," *Int. Commun. Heat Mass Transf.*, vol. 78, pp. 68–79, 2016.

[6] H. W. Xian, N. A. C. Sidik, S. R. Aid, T. L. Ken, and Y. Asako, "Review on preparation techniques, properties and performance of hybrid nanofluid in recent engineering applications," *J. Adv. Res. Fluid Mech. Therm. Sci.*, vol. 45, no. 1, pp. 1–13, 2018.

[7] J. Buongiorno, "Convective transport in nanofluids," 2006.

[8] R. K. Tiwari and M. K. Das, "Heat transfer augmentation in a two-sided lid-driven differentially heated square cavity utilizing nanofluids," *Int. J. Heat Mass Transf.*, vol. 50, no. 9–10, pp. 2002–2018, 2007.

[9] S. Reza-E-Rabbi, S. F. Ahmmed, S. M. Arifuzzaman, T. Sarkar, and M. S. Khan, "Computational modelling of multiphase fluid flow behaviour over a stretching sheet in the presence of nanoparticles," *Eng. Sci. Technol. an Int. J.*, vol. 23, no. 3, pp. 605–617, 2020.

[10] B. M. J. Rana, S. M. Arifuzzaman, S. Reza-E-Rabbi, S. F. Ahmed, and M. S. Khan, "Energy and magnetic flow analysis of Williamson micropolar nanofluid through stretching sheet," *Int. J. Heat Technol.*, vol. 37, no. 2, pp. 487–496, 2019.

[11] M. Khan, I. Karim, M. Rahman, S. M. Arifuzzaman, and P. Biswas, “Williamson fluid flow behaviour of MHD convective-radiative Cattaneo–Christov heat flux type over a linearly stretched-surface with heat generation and thermal-diffusion,” *Front. Heat Mass Transf.*, vol. 9, no. 1, 2017.

[12] S. P. A. Devi and S. S. U. Devi, “Numerical investigation of hydromagnetic hybrid Cu–Al2O3/water nanofluid flow over a permeable stretching sheet with suction,” *Int. J. Nonlinear Sci. Numer. Simul.*, vol. 17, no. 5, pp. 249–257, 2016.

[13] W. M. Rohsenow, J. P. Hartnett, and E. N. Ganic, “Handbook of heat transfer applications,” 1985.

[14] J. A. Masad and A. H. Nayfeh, “Effects of suction and wall shaping on the fundamental parametric resonance in boundary layers,” *Phys. Fluids A Fluid Dyn.*, vol. 4, no. 5, pp. 963–974, 1992.

[15] H. Rosali, A. Ishak, and I. Pop, “Micropolar fluid flow towards a stretching/shrinking sheet in a porous medium with suction,” *Int. Commun. Heat Mass Transf.*, vol. 39, no. 6, pp. 826–829, 2012.

[16] K. Hiemenz, “Die Grenzschicht an einem in den gleichformigen Flussigkeitsstrom eingetauchten geraden Kreiszylinder,” *Dinglers Polytech. J.*, vol. 326, pp. 321–324, 1911.

[17] F. Homann, “Der Einfluss grosser Zähigkeit bei der Strömung um den Zylinder und um die Kugel,” *ZAMM-Journal Appl. Math. Mech. für Angew. Math. und Mech.*, vol. 16, no. 3, pp. 153–164, 1936.

[18] C. TC, “Stagnation-point flow towards a stretching plate,” *J. Phys. Soc. Japan*, vol. 63, no. 6, pp. 2443–2444, 1994.

[19] C. Y. Wang, “Stagnation flow towards a shrinking sheet,” *Int. J. Non. Linear. Mech.*, vol. 43, no. 5, pp. 377–382, 2008.

[20] N. A. A. M. Nasir, A. Ishak, and I. Pop, “Stagnation-Point Flow Past a Permeable Stretching/Shrinking Sheet,” *Adv. Sci. Lett.*, vol. 23, no. 11, pp. 11040–11043, 2017.

[21] N. S. Khashi'ie, E. H. Hafidzuddin, N. M. Arifin, and N. Wahi, "Stagnation point flow of hybrid nanofluid over a permeable vertical stretching/shrinking cylinder with thermal stratification effect," *CFD Lett.*, vol. 12, no. 2, pp. 80–94, 2020.

[22] C. Y. Wang, "Fluid flow due to a stretching cylinder," *Phys. fluids*, vol. 31, no. 3, pp. 466–468, 1988.

[23] A. Ishak and R. Nazar, "Laminar boundary layer flow along a stretching cylinder," *Eur. J. Sci. Res.*, vol. 36, no. 1, pp. 22–29, 2009.

[24] V. Vinita and V. Poply, "Impact of outer velocity MHD slip flow and heat transfer of nanofluid past a stretching cylinder," *Mater. Today Proc.*, vol. 26, pp. 3429–3435, 2020.

[25] N. Najib, N. Bachok, N. M. Arifin, and A. Ishak, "Stagnation point flow and mass transfer with chemical reaction past a stretching/shrinking cylinder," *Sci. Rep.*, vol. 4, no. 1, pp. 1–7, 2014.

[26] N. S. Omar, N. Bachok, and N. M. Arifin, "Stagnation point flow over a stretching or shrinking cylinder in a copper-water nanofluid," *Indian J. Sci. Technol.*, vol. 8, no. 31, pp. 1–7, 2015.

[27] S. Nadeem, N. Abbas, and A. U. Khan, "Characteristics of three dimensional stagnation point flow of Hybrid nanofluid past a circular cylinder," *Results Phys.*, vol. 8, pp. 829–835, 2018.

[28] I. Waini, A. Ishak, and I. Pop, "Hybrid nanofluid flow towards a stagnation point on a stretching/shrinking cylinder," *Sci. Rep.*, vol. 10, no. 1, pp. 1–12, 2020.

[29] M. M. Maskeen, A. Zeeshan, O. U. Mehmood, and M. Hassan, "Heat transfer enhancement in hydromagnetic alumina–copper/water hybrid nanofluid flow over a stretching cylinder," *J. Therm. Anal. Calorim.*, vol. 138, no. 2, pp. 1127–1136, 2019.

[30] M. G. Reddy and K. V. Reddy, "Influence of Joule heating on MHD peristaltic flow of a nanofluid with compliant walls," *Procedia Eng.*, vol. 127, pp. 1002–1009, 2015.

[31] M. Sajid, S. A. Iqbal, M. Naveed, and Z. Abbas, "Joule heating and magnetohydrodynamic effects on ferrofluid (Fe3O4) flow in a semi-porous curved

channel," *J. Mol. Liq.*, vol. 222, pp. 1115–1120, 2016.

[32] Y. S. Daniel, Z. A. Aziz, Z. Ismail, and F. Salah, "Effects of thermal radiation, viscous and Joule heating on electrical MHD nanofluid with double stratification," *Chinese J. Phys.*, vol. 55, no. 3, pp. 630–651, 2017.

[33] L. Yan *et al.*, "Dual solutions and stability analysis of magnetized hybrid nanofluid with joule heating and multiple slip conditions," *Processes*, vol. 8, no. 3, p. 332, 2020.

[34] X.-H. Zhang *et al.*, "MHD stagnation point flow of nanofluid over a curved stretching/shrinking surface subject to the influence of Joule heating and convective condition," *Case Stud. Therm. Eng.*, vol. 26, p. 101184, 2021.

[35] M. N. Khan, "Thermal enhancement in hybrid nano-polymer using novel models for hybrid nanoparticles," *Case Stud. Therm. Eng.*, vol. 26, p. 101081, 2021.

[36] A. Jamaludin, K. Naganthran, R. Nazar, and I. Pop, "Thermal radiation and MHD effects in the mixed convection flow of Fe3O4–water ferrofluid towards a nonlinearly moving surface," *Processes*, vol. 8, no. 1, p. 95, 2020.

[37] I. Waini, A. Ishak, and I. Pop, "Flow towards a Stagnation Region of a Curved Surface in a Hybrid Nanofluid with Buoyancy Effects," *Mathematics*, vol. 9, no. 18, p. 2330, 2021.

[38] A. Abbasi *et al.*, "Optimized analysis and enhanced thermal efficiency of modified hybrid nanofluid (Al2O3, CuO, Cu) with nonlinear thermal radiation and shape features," *Case Stud. Therm. Eng.*, vol. 28, p. 101425, 2021.